Title	Diamond-like-carbon nanoparticle production and agglomeration following UV multi-photon excitation of static naphthalene/helium gas mixtures
Authors	Walsh, Anton J.;Tielens, A. G. G. M.;Ruth, Albert A.
Publication date	2016-07-11
Original Citation	Walsh, A. J., Tielens, A. G. G. M. and Ruth, A. A. (2016) 'Diamond-like-carbon nanoparticle production and agglomeration following UV multi-photon excitation of static naphthalene/helium gas mixtures', The Journal of Chemical Physics, 145(2), 024303 (12 pp). doi:10.1063/1.4955192
Type of publication	Article (peer-reviewed)
Link to publisher's version	10.1063/1.4955192
Rights	© 2016, AIP Publishing. This article may be downloaded for personal use only. Any other use requires prior permission of the author and AIP Publishing. The following article appeared in J. Chem. Phys. 145, 024303 (2016) and may be found at http://aip.scitation.org/doi/abs/10.1063/1.4955192
Download date	2025-02-05 04:47:44
Item downloaded from	https://hdl.handle.net/10468/3479

Diamond-like-carbon nanoparticle production and agglomeration following UV multi-photon excitation of static naphthalene/helium gas mixtures

A. J. Walsh' , A. G. G. M. Tielens, and A. A. Ruth'

Diamond-like-carbon nanoparticle production and agglomeration following UV multi-photon excitation of static naphthalene/helium gas mixtures

A. J. Walsh,[1,a)] A. G. G. M. Tielens,[2] and A. A. Ruth[1,b)]

[1]*Physics Department and Environmental Research Institute, University College Cork, Cork, Ireland*
[2]*Leiden Observatory, Leiden University, Niels Bohrweg 2, 2333-CA Leiden, The Netherlands*

We report the formation of nanoparticles with significant diamond character after UV multi-photon laser excitation of gaseous naphthalene, buffered in static helium gas, at room temperature. The nanoparticles are identified *in situ* by their absorption and scattering spectra between 400 and 850 nm, which are modeled using Mie theory. Comparisons of the particles' spectroscopic and optical properties with those of carbonaceous materials indicate a sp^3/sp^2 hybridization ratio of 8:1 of the particles formed. The particle extinction in the closed static (unstirred) gas-phase system exhibits a complex and quasi-oscillatory time dependence for the duration of up to several hours with periods ranging from seconds to many minutes. The extinction dynamics of the system is based on a combination of transport features and particle interaction, predominantly agglomeration. The relatively long period of agglomeration allows for a unique analysis of the agglomeration process of diamond-like carbon nanoparticles *in situ*. Published by AIP Publishing. [http://dx.doi.org/10.1063/1.4955192]

I. INTRODUCTION

Due to their unique physical and optical properties, nanodiamonds (NDs) have a large number of applications.[1–3] Their rich surface chemistry and large surface area make NDs an interesting nanocomposite.[4] The non-toxicity and mechanical stability of the diamond core make these composites appropriate for medical applications, such as drug delivery[5–7] and protein mimics.[8] Their strong mechanical and thermal properties, in addition to their surface versatility, make them excellent materials for lubrication.[9] Moreover, the fluorescence properties of nitrogen vacancy centers of NDs have opened up possible applications in high resolution magnetic sensing,[10] fluorescence resonance energy transfer,[11] and biomedical imaging.[12] In natural environments, NDs, with a small graphite fraction of ~10%, have been identified as presolar grains in meteorites.[13–15]

There are several techniques for the production of NDs,[1,16] including detonation synthesis,[2,17,18] milling of microcrystals,[19] pulsed laser ablation of graphite surfaces (in vacuum, in inert gaseous environments, or in liquids),[20] chemical vapor deposition (CVD),[21,22] and application of circular shockwaves.[23] Detonation synthesis is a popular commercially used technique.[1,3] The carbon and energy source are molecular explosives, which are placed in an oxygen deficient sealed chamber containing an inert gas or water. The explosives are ignited and 'soot-NDs' are formed. Detonation soot can consist of up to 80% diamond nanoparticles of typical sizes between 3 and 4 nm contained within submicron and micron size aggregates. The remainder of explosion products also contains graphitic carbon along with debris from the

chamber. Even though ND aggregates can be utilized in many areas, such as chromatography[24] and drug delivery,[25] generally de-agglomeration of these larger structures is required as well as purification in order to obtain viable NDs. Isolation of NDs, however, is generally not straightforward due to their strong agglomeration properties. A successful technique is to ground the ND powder together with micron-sized zirconium dioxide balls.[26] Oxidizing mineral acids at elevated temperatures are also commonly used to remove impurities on the surfaces and particles of up to 95% diamond content can be obtained.[1,3]

Diamond-like-carbon (DLC) materials are characterized by their significant fraction of diamond among graphitic carbon and/or hydrogenated amorphous carbon (a–C:H).[27,61] DLC materials possess many of the advantages that diamond exhibits, i.e., mechanical hardness, chemical and electrochemical inertness, and a large band gap. The main use of DLC materials has been in protective coatings of optical flats, magnetic storage disks, car parts, and biomedical appliances.[28]

In the present work, we report the formation of DLC nanoparticles, after UV multi-photon laser excitation of gaseous naphthalene buffered in static helium, at room temperature. The nanoparticles are identified *in situ* by their absorption and scattering profiles between 400 and 850 nm and modeled using Mie theory. Comparisons of their spectroscopic and optical properties with those of carbonaceous materials containing different sp^3/sp^2 hybridization ratios will be used to evaluate the prevalent sp^3/sp^2 ratio of the particles formed. As shown in Refs. 29 and 30, the particle extinction in this closed static (unstirred) gas-phase system exhibits complex and quasi-periodic oscillatory time dependence, which can persist for up to several hours. The extinction dynamics of the system is based on a combination of transport features and particle interaction, predominantly agglomeration. The relatively long period of agglomeration allows for a unique

---

a)Present address: Dutch Institute for Fundamental Energy Research, De Zaale 20, 5612 AJ Eindhoven, The Netherlands.
b)Author to whom correspondence should be addressed. Electronic mail: a.ruth@ucc.ie. Fax: +353-21-4276949.

analysis of the agglomeration process of DLC nanoparticles *in situ*.

In Section II, the experimental setup and previously observed results are briefly outlined; for a full description see Ref. 30. In Section III a (single) representative measurement is presented and analyzed in the spectral range 400-600 nm, demonstrating the production of DLC nanoparticles from UV multi-photon excitation of naphthalene, by comparison with spectral profiles of carbonaceous material, and the agglomeration of nanoparticles in the gas mixture. In Section IV, concurrent results in the spectral range 550-850 nm are presented. Formation routes to diamond-like material are discussed in Section V, followed by some conclusions and a brief outlook in Section VI.

II. EXPERIMENT

The experimental setup has been described in detail elsewhere,[29,30] and will only be briefly outlined here. The sample gas mixture is contained in a static gas chamber (volume ~5.3 dm^3), which can be evacuated to 10^{-3} mbar. Room temperature naphthalene vapour (0.06 mbar) is leaked into the evacuated chamber, proceeded by (grade 5) helium, typically at pressures above 5 mbar. Naphthalene (scintillation grade, >99% Aldrich, CAS 91-20-3) is exposed to focused UV light at 308 nm from a pulsed excimer laser (Lumonics EX-700, XeCl). Typically between 10 and 1000 pulses at repetition rates between 5 and 50 Hz are used, with average laser pulse energies ranging from 2 to 100 mJ. Optical losses over a ca. 10 mm cross-sectional area, perpendicular to the excitation pulse and through the focal point of the UV pulse, before and after UV excitation are measured using incoherent broadband cavity enhanced absorption spectroscopy (IBBCEAS).[31] Optical losses were measured with a spectral resolution of 1.65 nm and a temporal resolution as low as 10 ms in two wavelength regions: (a) 400–620 nm and (b) 550–850 nm. To calculate extinction using IBBCEAS the gas mixture of photo-products must be "well mixed" and the pathlength known. In the current measurements, extinction could not be extracted as the light interaction pathlength inside the cavity cannot be determined and may be time-dependent. Instead optical loss is characterized using αd, where α is extinction [cm^{-1}] and d is pathlength [cm].

III. RESULTS

After UV photo-excitation the system exhibits a variety of dynamic behaviour in optical losses, and under certain conditions (quasi-)oscillations could be observed for up to several hours.[29,30,32] A sample time-dependent optical loss measurement at 550 nm is shown in Figure 1. After an initial short period where no discernible pattern is observed, the optical loss begins to oscillate and continues for over an hour.

Spectra recorded during dynamic behaviour are unstructured, increasing monotonically with decreasing wavelength in both the 400-620 nm and 550-850 nm regions, see Figure 2. A general broad (weak) feature between ca. 660 and 810 nm appears in virtually all spectra. The general lack of isolated
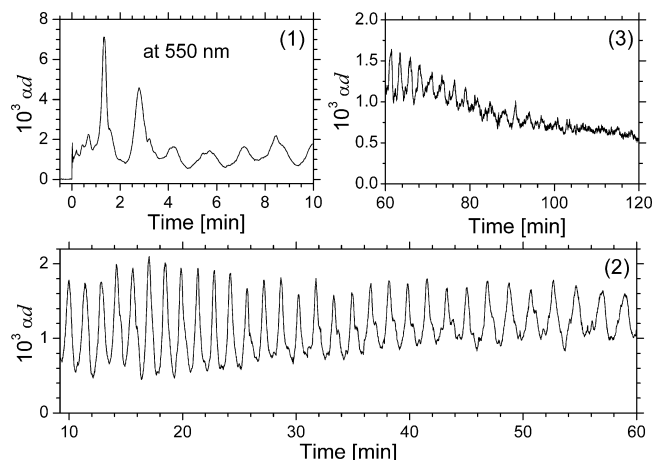

FIG. 1. Time-dependent optical loss at 550 nm of the UV photolysis products of gaseous naphthalene in 50 mbar of helium at room temperature (photolysis conditions: 35 UV pulses of average energy 24 mJ at 10 Hz (pulse duration ~10 ns); the last photolysis pulse denotes time $t = 0$ min in view graphs). The first 10 min following the multiphoton excitation is shown in panel (1), where no discernible pattern can be observed for the initial ca. 4 min. Subsequently the optical loss begins to oscillate, shown in panel (2), with quasi-periods of ca. 2 min. Oscillations occur for approximately 1.5 h. After 2 h the optical losses had not returned to zero, shown in panel (3).

features demonstrates that the optical losses are not solely based on absorption, but contain an important contribution by scattering. Although missing isolated spectral features, a change in the wavelength dependence of extinction could
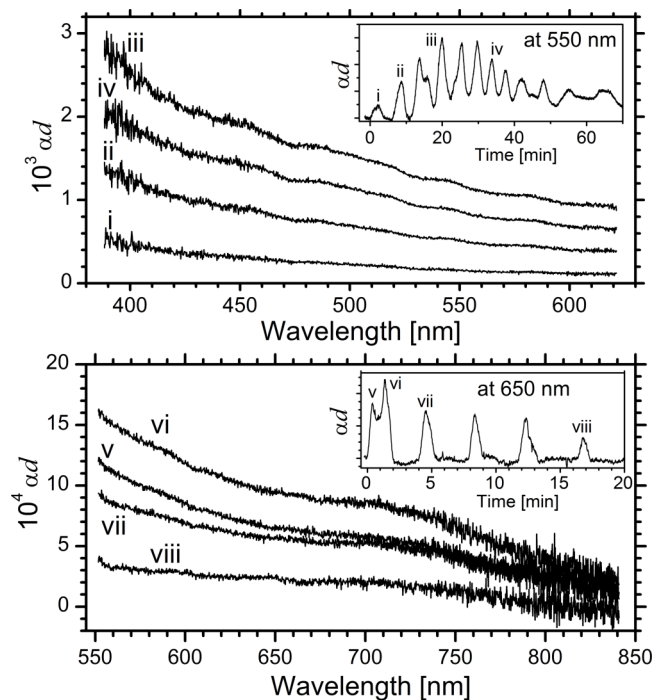

FIG. 2. Sample αd spectra measured in two wavelength ranges. The top and bottom panels display four spectra each, measured in the wavelength ranges 380-620 nm and 550-850 nm, respectively. The insets display the temporal quasi-oscillatory change in αd at a single wavelength, 550 nm (top panel) and 650 nm (bottom panel). Each spectrum was recorded at maximal αd during oscillations and is labelled (i), (ii), . . . , (viii) in both panels and insets. UV excitation occurred at 0 min. Conditions of both measurements are described in full in Ref. 30.
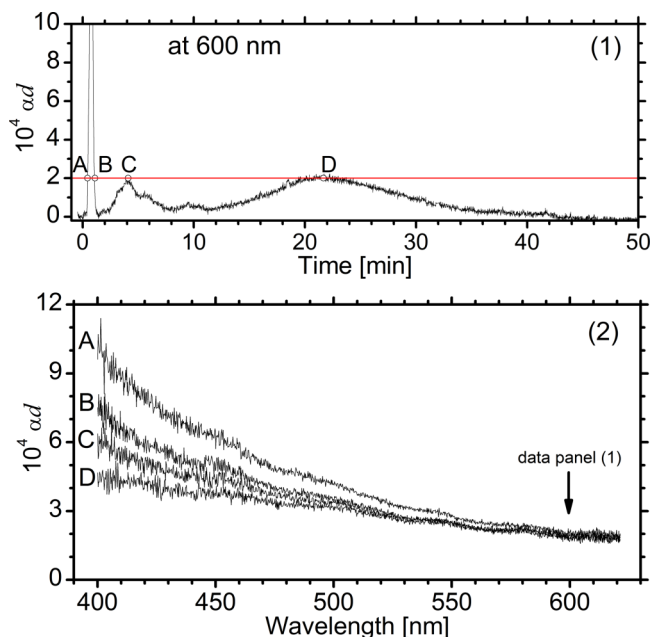
FIG. 3. (1) Time-dependent measurement of optical loss, αd, at 600 nm. (2) αd spectra measured at times marked A, B, C, and D in panel (1). Note: Spectra have the same value at ~600 nm as indicated by the dashed line in panel (1). (See text for more details.)

be observed over time, see Figure 3. This change indicates that the time-dependent behaviour cannot be described solely by dynamic transport of photolysis products in the chamber. Particle growth and/or interactions also play a significant role and consequently the size distribution of particles is also time-dependent, see Sections IV C and IV D.

Although it was possible to qualitatively predict the type of dynamic behaviour for different pressure regimes of the buffer gas,[29] it was impossible to predict the wavelength dependence of optical spectra at a particular time. However, the evolution of wavelength dependence of spectra, for the majority of measurements, showed similar behaviour. Spectra recorded closest to UV photolysis exhibited the strongest wavelength dependence (Section IV B), i.e., a significant increase of extinction towards the UV and as time evolves the strong wavelength dependence is reduced and the extinction gradient towards the UV decreases. This dynamic spectral behaviour was observed, to varying degrees of change and at different rates, in virtually all measurements and no behaviour to the contrary was observed.

An important aspect of the observed dynamics is particle deposition on the chamber walls, which acts as a sink for particles generated in the photolysis. Thus the distance of the UV pulse focus from the chamber walls for a given buffer gas pressure was found to have an influence on the observed dynamics. By reducing the volume of the chamber, such that the distance from the focus to the nearest wall surface is 5 cm or less, no oscillations are observed and the time-dependent αd behaviour simplifies into a single increase in optical loss followed by decay.[29] As particles are removed from the gas mixture over time by depositing on the chamber walls, changes in optical losses cease and return to zero much faster under "small volume" conditions. When the observed loss

was no longer time-dependent, it was possible in some cases to resume oscillatory αd behaviour by heating the chamber walls.

IV. DESCRIPTION OF SPECTRA USING MIE THEORY

The absorption and scattering of electromagnetic radiation of light by spherical particles, of size similar to the wavelength of light, can be calculated using Mie theory. For a full description of Mie theory, including formalism used in all computations here, see Ref. 33. To apply Mie theory we assume particles to be spherical and the total extinction of the particles inside the chamber to be equal to the sum of intensities scattered and absorbed by individual particles. To calculate extinction, the size distribution of particles and their complex refractive index, n, are required. In this section, these parameters are retrieved for particles formed in a relatively simple time-dependent extinction measurement, with only 3 extinction maxima. The behaviour of particle dynamics found in this measurement is common in the vast majority of cases. Sample measurement details are described in Section IV A. For analysis, the measurement is divided into two periods, occurring in the initial 30 s after UV excitation and the following dynamic behavior over the following 50 min. In Section IV B, the first period is analyzed. An appropriate wavelength dependent complex refractive index is retrieved, using values reported in the literature for other carbon materials, along with a single particle size distribution. In Section IV C, a suitable size distribution and complex refractive index for the rest of the measurement is determined, using parameters retrieved in Section IV B.

A. Example measurement

A representative time-dependent loss measurement (αd) at 600 nm and loss spectra between 400 and 620 nm, taken at four times, (A) 0.42 min, (B) 1.1 min, (C) 4.2 min, and (D) 19.2 min, after laser excitation are shown in panels (1) and (2) of Figure 3, respectively. The experiment was performed at an ambient temperature of ca. 34.5 °C and with a helium buffer gas pressure of 10 mbar. 35 UV light pulses at 10 Hz and an average energy of 16.3 mJ were focused into the centre of the chamber. The laser's temporal and spatial full width at half maximum (FWHM) are estimated as 15 ns and 50 μm, respectively. This results in an on-axis peak irradiance of ca. 1.38 GW/cm². An initial first maximum of $\alpha d = 0.002$ is observed 1.4 min after photo-excitation. This initial peak was followed by 2 more maxima over a 45 min period. The last broad increase and decrease in αd occurred over a ca. 15 min period. At times A to D (see panel (1) of Figure 3), the optical loss at 600 nm is approximately the same ($\alpha d \approx 2 \times 10^{-4}$). However, the wavelength dependence of αd is not comparable; over time the optical loss at shorter wavelengths decreases.

B. Analysis of extinction spectra immediately after UV excitation

The laser pulse produces a mixture of naphthalene fragments formed from multi-photon absorption,[30] which are

the precursors for chemical growth. The growth is governed by the cooling of the "warm" gaseous species; the collision rate depends on the initial temperature and pressure at which precursor species were generated. The time scale of chemical growth cannot be determined by way of the present setup, owing to a limited time resolution, or wavelength range, or both. The variety of time scales at which optical losses appear has been described previously in Refs. 29 and 32 (also see Section IV C). However, approximately 30 s after UV excitation the dominant source of optical loss is due to absorption and scattering by particles (see spectrum A in panel (2) of Figure 3). In other words, after that initial time period of ~30 s, where no information on the nature of the loss can be obtained using our current approach, IBBCEAS is an adequate method to monitor the subsequent agglomeration phase.

The initial chemical growth period (~30 s) is followed by agglomeration on a time scale of ca. 50 min, accompanied by a loss of particles and aggregates to the chamber wall. This period is characterized by dynamic motion of the particle and aggregate cloud in the chamber, which may be potentially driven by the initial heating effect caused by the laser pulse, leading to the observed oscillatory behavior.

The wavelength dependence of the extinction is dominated by the material properties (i.e., optical constants). For small grain sizes (i.e., $2\pi r/\lambda \ll 1$, where r is the particle radius and λ is light's wavelength) the extinction's wavelength dependence ($\sim\lambda^{-4}$) is largely independent of the actual size, known as the Rayleigh range. Increasing the grain size will generally cause the extinction to become less dependent on wavelength ($\sim\lambda^{-a}$, with a being typically between 1 and 2). For the description of extinction dynamics of the system, we assume that the initial distribution of particles after photolysis is likely to be the narrowest. Particle interaction and agglomeration would naturally lead to a broadening or other more complex changes of the size distribution over time. Consequently, to model the wavelength dependence of the measured extinction *in the initial phase*, we approximated the distribution as a single primary particle size of diameter D at 30 s after photo-excitation. We also assume a pathlength of 1 cm for the calculation of extinction (required in IBBCEAS), based on the hypothesis that particles are situated in the chamber centre around the photolysis area. Note that a change in the pathlength will not affect the particle size distribution; however, it will result in a linear change in particle number density. Lastly, a common wavelength dependent complex refractive index must be selected. The ratio of sp^3 to sp^2 hybridized carbon bonds present is used to characterize the carbon material. Graphite consists purely of sp^2 hybridized bonds and diamond purely of sp^3 hybridized bonds. Selection of a complex refractive index is the main source of error in using extinction to determine particle size, as the refractive index is extremely sensitive to the particle formation pathway. However, although error in refractive index selection leads to inaccuracy, the observation of trends and changes is not affected.

An optimization program containing the two independent parameters, size and number density, was utilized. The

program was based on the Nelder-Mead simplex algorithm of Mathematica 8.[34] A number of fits using a variety of complex refractive indices, obtained under different conditions and containing contrasting sp^3/sp^2 ratios, were performed. For optimization of simulated spectra in comparison to measured spectra, equidistant data points between 400 and 600 nm (50 nm apart) were selected. In total five data points turned out to be adequate for the optimization due to the featureless nature of the optical properties of carbonaceous particles. Optimization in the initial phase was performed on spectrum A in panel (2) of Figure 3, using the complex refractive index of carbonaceous material formed in a flame, in pyrolysis of cellulose, through sputtering of graphite in an argon plasma and an argon/hydrogen plasma. Specifics of those carbonaceous system are outlined and discussed in Subsections IV B 1–IV B 4.

1. Soot

The consistency of particulate matter formed from polycyclic aromatic hydrocarbons (PAHs) has been studied in connection with soot formation in combustion processes, where PAHs act as precursors for soot formation. Soot carbon bonds are considered to be dominated by sp^2 bonds and in Walsh *et al.*,[30] we suggested the path to particle formation follows a similar path to soot formation.[35,36] However, no good comparison could be found between the optical properties of flame soot and spectra measured immediately after UV photolysis. Panel (1) of Figure 4 shows an optimal simulation of spectrum A in panel (2) of Figure 3, using the complex refractive index of flame soot determined by Chang
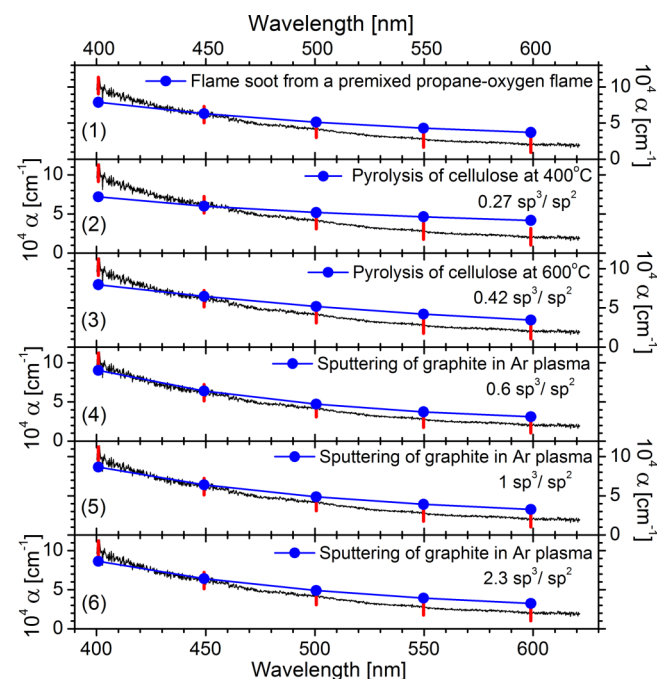

FIG. 4. Black trace: Measured spectrum. Blue trace and blue dots: Fit to extinction spectra measured at time marked A in panel (1) of Figure 3, assuming different carbonaceous materials with sp^3/sp^2 ratios of up to 2.3, and a single particle size. Fit parameters are summarized in Table I. Red vertical lines: Pivot points for the fit.

TABLE I. Fit results for varying sp^3/sp^2 ratio, using a single particle size (diameter D) and the Mie approximation. The minimum least square sum, χ^2, represents the quality of the fit and is based on the sum of squares of the difference between simulation and measurement. The experimental data are best reproduced with an sp^3/sp^2 ratio of ≈ 8.1 and $D = 35$ nm.

sp^3/sp^2	$\chi^2/10^{-8}$	D (nm)	Reference
Soot	11	96	37
0.27	18	56	38
0.42	10	25	38
0.6	3.6	116	40
1	5.5	120	40
2.3	5.7	137	40
4	0.3	104	40
8.1	0.05	35	40

and Charalampopoulos[37] from a premixed propane-oxygen flame. The corresponding output parameters, i.e., the single particle diameter D and χ^2 representing the quality of the fit, are shown in Table I. The description is poor and unable to describe the substantial rise of extinction towards the UV.

2. Pyrolysis of cellulose

Jäger *et al.* studied structurally different amorphous carbonaceous dust analogues with different sp^3/sp^2 ratios.[38] The materials were synthesized by pyrolysis of cellulose at 400, 600, 800, and 1000 °C, with hybridization ratios decreasing with increasing temperature. The complex refractive index of the materials was determined by using reflectance of bulk samples between 0.2 and 500 μm and Kramers-Kronig analysis. The two best simulations of spectrum A using complex refractive index pertaining to the pyrolysis of cellulose at 400 °C and 600 °C (approximately 20% and 30% of the carbon bonds are sp^3, respectively) are shown in panels (2) and (3) of Figure 4. The corresponding output parameters are given in Table I. Similar to simulation using parameters for soot, the agreement is inadequate for cellulose-based materials.

3. Sputtering of graphite in argon plasma

Savvides[39] reported the formation of DLC materials on films using unbalanced magnetron gun sputtering of a graphite target in argon plasma. The wavelength dependent refractive index was calculated from reflectance and transmittance data of the materials. The sp^3/sp^2 ratio varies as a function of ion energy per deposited carbon atom. Using purely carbon atom deposition, up to 70% sp^3 bonds could be achieved. Panels (4)–(6) of Figure 4 show simulations using refractive indices from higher sp^3/sp^2 bond ratios as reported by Savvides.[40,41] The simulations with parameters for pure carbon material agree somewhat better with our measurement, however, the agreement with the observed spectral dependence is inadequate, especially towards the UV where a significant rise in extinction loss is not reproduced well (cp. Table I and Figure 4).

4. Sputtering of graphite in argon/hydrogen plasma

Higher sp^3/sp^2 bond ratios, up to 89% sp^3 bonds, were reported in carbon film deposition from argon/hydrogen plasmas which produce DLC films.[40,41] Panels (1) and (2) of Figure 5 show fits using the complex refractive indices of DLC, with 80% and 89% sp^3 bonds. By using the optical properties of DLC materials, spectrum A in panel (2) of Figure 3 can be reproduced satisfactorily. The fit based on properties of 89% sp^3 bonds containing 25% hydrogen leads to the best agreement (cf. Table I and Fig. 5). The retrieved particle diameter of 35 nm, using 89% sp^3 bonds, is near the Rayleigh range. Consequently it is impossible to determine if particles of smaller dimensions are formed during photolysis, as there is no significant dependence on size in the optical spectrum.

In the DLC films reported in Refs. 40 and 41 the only other species present is hydrogen at ~25%. This percentage of hydrogen cannot be explained through CH passivation bonds on the surface of the film alone. Hence hydrogen should also occur inside the carbon film where the small fraction of sp^2 carbon sites is probably paired up into at least ethylenic units. In the nanoparticles, however, the overall percentage of CH bonds present could not be determined from the present measurement and compared with sp^3 and sp^2 bonds, as their spectral features do not sufficiently influence the spectrum between 400 and 600 nm. Moreover, an overestimation of the sp^3/sp^2 ratio is reported in Ref. 28 which is based on work similar to that in Ref. 40. Critically evaluating the correctness of the hybridization ratio is not possible based on the information given concerning the discrepancy between Refs. 28 and 40. However, it is clear from Table I that an increasing sp^3/sp^2 ratio continually correlates with improving the fits. Consequently, the largest sp^3/sp^2 ratio of ~8.1 has been taken as a good approximation for DLC nanoparticle formation immediately after UV photolysis.
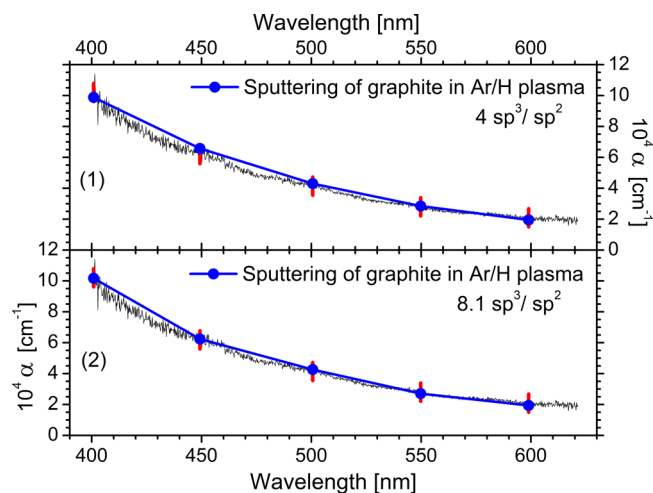

FIG. 5. Black trace: Measured spectrum. Blue trace and blue dots: Fit to extinction spectra measured at time marked A in panel (1) of Figure 3, assuming DLC materials with sp^3/sp^2 ratios of 4 in panel (1) and of 8.1 in panel (2). A single particle size was used in the corresponding model. Fit parameters are summarized in Table I. Red vertical lines: Pivot points for the fit.

Since typical optical band gaps between 0.5 and 3 eV are stated,[40] we investigated the possibility of using Tauc plots[42] to potentially further elucidate the nature of the DLC particles formed in the photolysis. Based on the data in panel (2) of Fig. 3, trace A, the band gap as per a corresponding Tauc plot could be between ca. 1 and 2 eV. That band gap range would indicate amorphous DLC (i.e., a–C:H) according to Table 1 in Ref. 28. This conclusion is, however, to be looked at with great caution, as Tauc plots are usually applied to thin films and not to gas-phase particle suspensions. Moreover, the spectral region between 400 and 600 nm is small, so that the Tauc extrapolation results in rather large uncertainties.

C. Analysis and simulation of extinction measured at times greater than 30 s

As no distinguishable features appear and/or disappear in the spectra as a function of time, and due to the inertness and mechanical stability of DLC, chemical reactions are expected to be insignificant for the dynamics of the system after 30 s of UV excitation. Consequently, the evolution of spectra is likely to be solely governed by particle interaction. The dominant process of change is expected to be agglomeration, due to the mechanical stability of DLC. The period >30 s is characterized by dynamic motion of particle and aggregate clouds in the chamber, which is probably due to the heating effect caused by the initial laser excitation pulses, accompanied by a loss of particles and aggregates to the chamber wall.

For the modeling of particle size, a normal distribution on a logarithmic scale was used

$$N_{\log}(x) = \frac{A}{\sigma\sqrt{\pi/2}} \exp\left[-\frac{(x-x_0)^2}{2\sigma^2}\right], \quad (1a)$$

where the unitless size variable

$$x = \log_{10}(D), \quad (1b)$$

the amplitude factor, A, the standard deviation, σ, and size at maximum, x_0, are independent parameters; D represents the particle diameter in nanometers. The log-normal distribution is widely used to empirically describe distributions, both man-made and natural, and it allows for analysis over several orders of magnitude. The continuous log-normal distribution is divided into discrete particle sizes using 13 equally spaced size bins placed between −2.5 σ and +2.5 σ in the log-normal distribution. The extinction efficiency of the particles assigned to each size bin is approximated by using the extinction efficiency of the mid-particle size of each size bin. Using 13 size bins was found to be sufficient to optimize the model fit. The most probable size of the log-normal distribution (center value of the maximum) is set at $x_0 = \log_{10}(35 \text{ nm})$ for the entire time duration of the measurement. This implies that the small particles formed immediately after UV photolysis remain the most abundant throughout the measurement; their sizes are the most likely to occur even though the system evolves in time. The agglomeration of particles over time is described by the *increasing* width of the size distribution and consequently decreasing concentration of particles of size $D = 35$ nm.

The effective description of agglomerates can vary with formation pathway, ranging from diffusion flames to the interstellar medium, consequently many models are available. In the current set-up, fractal aggregates are not expected.[43] Hence we assumed the particle agglomerates to be rather compact with a certain space filling factor (further discussed below). The agglomerates can be characterized as an inhomogeneous material containing DLC and pores, resulting in a varying refractive index throughout the medium. Consequently, the Bruggeman *effective medium approximation* (EMA) is used to determine an effective refractive index for the agglomerates.[44] The Bruggeman EMA approximates the material as a random mixture of spherical particles, DLC and pores in the present case, embedded in an effective medium. Using this approximation, an effective dielectric constant, ε_{eff}, can be extracted from

$$f_{\text{DLC}}\left(\frac{\varepsilon_{\text{DLC}} - \varepsilon_{\text{eff}}}{\varepsilon_{\text{DLC}} + 2\varepsilon_{\text{eff}}}\right) + f_{\text{pores}}\left(\frac{\varepsilon_{\text{pores}} - \varepsilon_{\text{eff}}}{\varepsilon_{\text{pores}} + 2\varepsilon_{\text{eff}}}\right) = 0, \quad (2a)$$

$$f_{\text{DLC}} + f_{\text{pores}} = 1, \quad (2b)$$

where ε_{DCL} and $\varepsilon_{\text{pores}}$ are the dielectric constants of DLC and pores, respectively, and f_{DCL} and f_{pores} are their respective filling factors. The complex refractive index of the effective medium can then be calculated using the relation $n_{\text{eff}}^2 = \varepsilon_{\text{eff}}$. The dielectric constant of the pores is taken to be that of vacuum, i.e., $\varepsilon_{\text{pores}} = 1$. The filling factor is chosen from the Ballistic Particle-Cluster Aggregates (BPCA) model of Kozasa *et al.* for compact agglomerates, where the DLC particles are considered as projectiles onto the agglomerates, with a sticking probability of one.[45] Using the BPCA model the filling factor of DLC is taken to be $f_{\text{DCL}} = 0.85$.

Retrieved parameters of fits to spectra B, C, and D are given in Table II. Figures 6–8 show fit results for spectra B, C, and D, respectively. In each figure panel (1) shows the extinction spectra (black line), pivot points used for optimization (red marks), and the simulated spectra (blue solid circles connected by line). Panels (2) show the following parameter f:

$$f = \frac{N_D}{D'' - D'}, \quad (3)$$

where N_D is the concentration of particles in the size bin represented by diameter D, and D'' and D' are the boundaries of the corresponding relative size bin. Panels (3) in Figures 6–8 show the contribution of particles in each size bin to the total extinction. In all three measurements it was found that particles of diameters less than 35 nm do not contribute substantially to the total extinction. Consequently, details of the smallest size

TABLE II. Parameters retrieved from fits to the spectra measured at times B, C, and D (cf. panel (1) of Figure 3), using a porous DLC material, with sp^3/sp^2 ratio of 8.1, the Bruggeman EMA, a filling factor of 0.85, and a log-normal distribution. The minimum least square sum, χ^2, represents the quality of the fit and is based on the sum of squares of the difference between simulation and measurement.

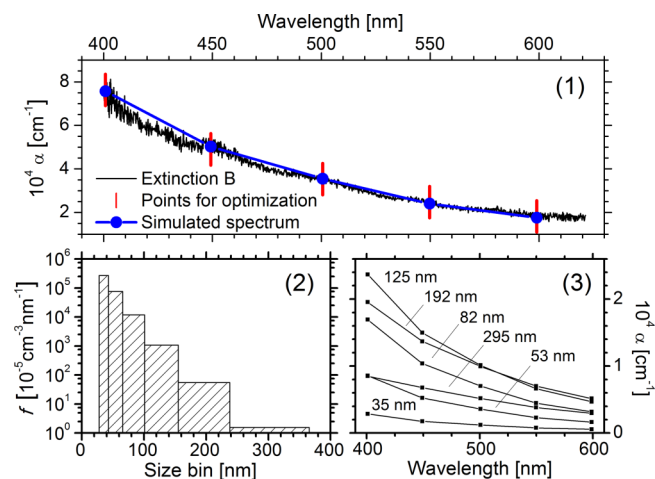| Spectrum	Time (min)	$\chi^2/10^{-8}$	σ	$A/10^{-7}$ (cm^{-3})
B	1.1	0.027	0.48	54
C	4.2	0.002	0.59	13
D	19.2	0.067	0.66	5

FIG. 6. (1) Fit to extinction measured at time B marked in panel (1) of Figure 3 using a porous DLC material, with sp^3/sp^2 ratio of 8.1, the Bruggeman EMA, a filling factor of 0.85, and a log-normal distribution. (2) Particle concentration per size bin f for each size bin, representing the log-normal distribution of particle size. (3) Contribution of particles in each size bin to the total extinction.

FIG. 8. (1) Fit to extinction measured at time D marked in panel (1) of Figure 3 using a porous DLC material, with sp^3/sp^2 ratio of 8.1, the Bruggeman EMA, a filling factor of 0.85, and a log-normal distribution. (2) Particle concentration per size bin f for each size bin, representing the log-normal distribution of particle size. (3) Contribution of particles in each size bin to the total extinction.

bins have been omitted from Figures 6–8. Similarly, the size of the largest particles in the fit to spectrum B does not contribute significantly to extinction and has been omitted from Figure 6. As illustrated by the results in Table II and Figures 6–8, the Bruggeman EMA and Mie theory are adequate to describe the time-dependent behavior of the extinction spectra for porous carbon material containing 8.9% sp^3 bonds and using a 0.85 filling factor. The description is reasonably simple and physically meaningful.

As anticipated for agglomerating particles, the width σ of the log-normal distribution increases with time. Hence the largest particle size, of diameter ∼1142 nm, was retrieved from spectrum D in a very low concentration. Spectra B and C were measured at 1.1 min and 4.2 min, i.e., within the first 5 min after UV excitation. In this time frame σ increased by ca.
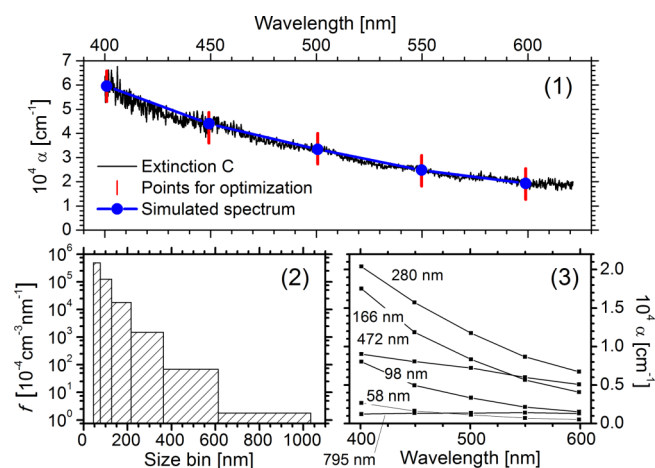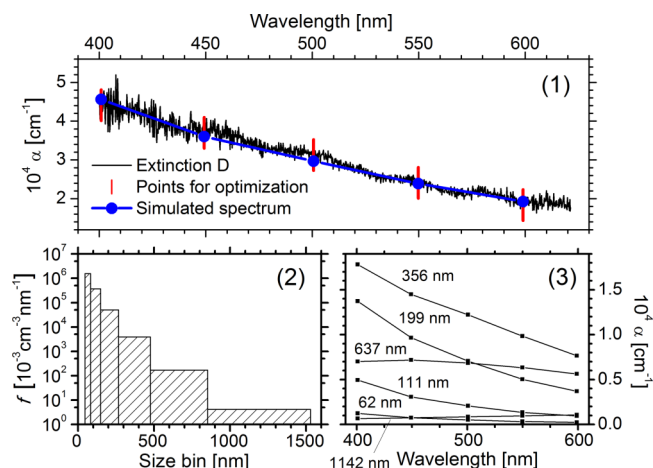
22%. Spectrum D was measured ca. 15 min after spectrum C, however, the width increased by almost half, i.e., 11.5%. The change in the rate of agglomeration of particles is likely due to, first, the reduction in the particle number density owing to the expansion of the cloud, second, to the agglomeration process itself and, third, to adsorption losses on the chamber walls. These processes make the initial agglomeration rate time-dependent and thus it is difficult to identify the size of nanoparticles formed from the chemical reaction scheme immediately after a single UV excitation pulse. The 10 ms time resolution of the IBBCEAS setup is not high enough to study the chemical route to DLC formation. Moreover, as the spectral dependence is very close to the Rayleigh range for a spectrum of nanoparticles with $D = 35$ nm, nanoparticles of diameters less than this will not significantly contribute to a change in the wavelength dependence of optical losses.

Within ∼20 s after photo-excitation, no change in optical loss is observed. This phenomenon also occurred in other measurements, previously described in Ruth *et al.*[29] It is likely that in this time frame particles have already formed, as energy has dissipated and radicals would react much faster at the pressures of the experiments. However, the particle size is expected to be small (<35 nm) causing only a small extinction. Consequently, although there is a high density of particles, their combined extinction is below the sensitivity of the setup. Only after agglomeration, the absorption and scattering by particles will become observable. The delay in the observation of optical losses may be due to a small and gradually increasing rate of agglomeration.

D. Characteristics of the 550-850 nm range

The dynamic behaviour of spectra in the 550-850 nm range was qualitatively the same as in the 400-620 nm range, i.e., with increasing measurement time the generally larger extinction in the UV decreased, concurrent with measurements made in the 400-620 nm range.[30] Unlike spectra in the 400-620

FIG. 7. (1) Fit to extinction measured at time C marked in panel (1) of Figure 3 using a porous DLC material, with sp^3/sp^2 ratio of 8.1, the Bruggeman EMA, a filling factor of 0.85, and a log-normal distribution. (2) Particle concentration per size bin f for each size bin, representing the log-normal distribution of particle size. (3) Contribution of particles in each size bin to the total extinction.

nm range, spectra in the 550-850 nm range contain a broad feature located between ~660 and ~810 nm. The source of this (potentially molecular) feature could not be identified. A similar broad feature, with maximum in the 720-730 nm range, has been observed in hydrogen rich diamonds.[46] However, the feature was also not identified. Strong absorption features in the 510-580 nm range are also observed in diamond,[47] which have been suggested to be due to nickel defects, through photoluminescence studies. Features in that region were not present in our spectra. Reactions with traces of O_2 or N_2 at partial pressures below 10^{-3} mbar cannot be excluded *per se*, however, there is no evidence for their occurrence. A meaningful model to simulate spectra in the 550-850 nm is difficult to establish without identification of the source of the feature. Thus, only the spectra in the 400-620 nm region were used for the determination of the sp^3/sp^2 bond ratio in this study.

E. Investigations outside 400-850 nm range

Optical properties outside of the 400-850 nm range can add further understanding to the DLC material. Further, Tauc plot analysis can potentially help determining the optical gap and C/H ratio of the nanoparticles. IR spectra can also reveal significant details of the hydrogen content, as well as possible minor contaminants, due to the strong dipole moment of bonds such as CO in the IR. However, the gas phase nature of the setup, the lifetime of the DLC nanoparticles formed, before agglomeration begins, and the dynamic behavior of products, currently stand in the way. Collection of DLC nanoparticles, near the focus, allows mobility of the DLC nanoparticles for different tests. However, the size distribution of particles evolves, making *ex situ* observations difficult. Collection of particles can also result in agglomeration, resulting in distortion of the nanoparticles' individual characteristics. Comparison of extinction using the optical properties of finite sized materials calculated from a model solely dependent on the optical gap will be the focus of future work. Finally, polarization effects would have been rather interesting to investigate in order to obtain more information on the nature of the photolysis products formed. However, polarization effects are difficult to measure in cavity experiments, as the polarization state of light is altered by the cavity. Hence this was not attempted.

V. POSSIBLE ROUTES OF DLC FORMATION

The formation of DLC nanoparticles with the current approach is unique and no data on similar synthesis procedures of nano-sized DLC materials could be found in the literature. The dynamics of local pressure and temperature following multi-photon excitation, and the generation of specific fragments, ions, and radicals will have an influence on particle formation. Even though PAHs are generally remarkably photo-stable, dissociation energies in neutral and in ionic naphthalene can be assumed to be similar[48,49] (about 4.5 eV for H-loss). In the present case, where UV

excitation is at 308 nm, fragmentation can in principle occur upon 2-photon excitation in neutral naphthalene or upon 4-photon excitation (or higher) via cationic naphthalene. There is evidence that multi-photon excitation ($n > 3$) does indeed occur in our experiment.[30,32] Due to this fact and owing to the very limited information about the potential fragmentation of neutral naphthalene, ionic fragmentation will be considered here. The main cationic fragmentation channels of naphthalene after photo-excitation have been identified in previous studies[50–53] due to their importance in soot formation and potentially for the development of species in the interstellar medium. The ion fragmentation channels can be divided into a group at lower (<16 eV) and higher (>18 eV) excitation energy. All low energy channels, which dominate the fragmentation of naphthalene, are energetically possible upon 4-photon excitation in the present experiment (16.1 eV). The most prominent low-energy fragmentation pathways comprise –H (15.35 eV), –H_2 (15.60 eV), and –C_2H_2 loss reactions.[50] The complete photodestruction of the naphthalene cation is suggested to proceed via subsequent C_2H_2 loss: $C_{10}H_8^+ + h\nu \rightarrow C_{10}H_8^+ - n(C_2H_2)$ with (n = 1...4).[54]

In our previous work,[30] we suggested a likely chemical pathway to particle formation to be through the growth of PAHs. Even though there are a number of possible scenarios and models of reaction pathways for nascent soot formation from PAHs[35] (e.g., through resonantly stabilized free-radical species), we assumed the widely established process of Hydrogen Abstraction Carbon Addition (HACA),[36,55] which essentially captures the thermodynamic and kinetic requirements for the sooting process. HACA is used to describe the first steps in soot formation to masses of ca. 500-1000 amu. This phase of growth is followed by a nucleation process of gaseous species leading to solid particles (up to ca. <1.5 nm), which finally start to coagulate. As soot contains a low diamond content, the chemical mechanism of growth through PAHs is highly unlikely.

DLC can be formed from phase transition, graphite to diamond, and by chemical reaction schemes.[28] High temperature (>2000 K) and pressure (~10 GPa) are required for the phase transition to occur. In shockwave synthesis of NDs, the high temperature created in the shockwave is key for the formation of diamond structure. In the current setup, a shockwave is created by a single UV pulse at low pressure. However, the estimated upper limit of local temperature is less than 500 K based on the excitation conditions.[29] This value was evaluated assuming a 5-photon energy conversion per absorbing naphthalene molecule in 80 mbar of helium.[29] A temperature of only 500 K is far below the requirement for diamond to be formed through a phase transition.

For detonation synthesis of NDs, the formation pathway is still debatable. Both models of phase transition, where the diamond is formed during the detonation wave,[56] and chemical pathway, where the detonation wave forms the chemical precursors necessary for diamond growth,[18] have been suggested. For chemical growth mechanisms, temperatures of less than 1000 K and pressures between 1 kPa and 100 kPa are required. These are conditions that are comparable with those in the experiments presented here, i.e., possible local temperatures of up to 500 K and the presence of chemical

precursors which are generated from fragmentation during UV excitation. These conditions are also comparable to diamond growth on films, by chemical vapor deposition (CVD) and plasma-enhanced CVD.

Although the time scale of DLC formation is not known for the current experiments, the conditions are not dissimilar from detonation synthesis of nanodiamonds, i.e., initiation through the release of energy on a nanosecond scale (the laser excitation pulse) and the resulting shockwave. Since a plasma plume is created from the UV excitation, comparison can also be made with plasma-enhanced CVD. Similar to plasma-enhanced CVD (which is used to describe detonation synthesis), the present approach resembles models of nanodiamond formation via a chemical pathway. The growth of DLC from plasma-enhanced CVD can follow (a) physical, or (b) chemical processes.[28]

(a) Subsurface implantation of carbon containing ions into the bulk of the carbon material, followed by preferential formation of sp^3 bonds, is a *physical process* that is based on, and well described by, numerical and analytical models. However, the entire mechanism is not fully understood, in particular the method of relaxation, which is suppressed at high ion energy and temperature.[28] For a pure carbon plasma, the highest sp^3 fractions are formed by C^+ ions with energy around 100 eV. For a hydrogen containing plasma, the molecular ions incident on the surface will break up into atomic ions and each ion will penetrate into the bulk. In the experiments, subsurface plantation is unlikely to play a large role in diamond formation. The carbon ion energy range of interest for the process is between 10 and 1000 eV. Pure carbon ion formation from naphthalene was not observed by Jochim *et al.*[48] by UV excitation of more than 22 eV. The low energy available to molecular ions formed from UV excitation make fragmentation unlikely upon collisions.

(b) In *chemical processes* of plasma-enhanced CVD,[22] reactions can occur on the surface, or in the bulk. In the plasma above the surface, reactions between the source hydrocarbon, usually methane, and hydrogen atoms create a mixture of hydrocarbon species, including reactive carbon containing radicals. The addition of species to particle nuclei is dependent on their probability to stick to the CH covered surface. Di-radicals and unsaturated species, such as C_2H_4 and C_2H_2, can insert directly into the surface CC and CH bonds, and these species play the most important role in growth. Of these neutral species, C_2H_2 is the most likely to be abundant in the present gas mixture, due to the naphthalene fragmentation patterns below 16 eV.[48] Successive abstraction of C_2H_2 has also been suggested by Ekern *et al.*[54] to be the dominant pathway for the full destruction of the naphthalene cation.

Atomic hydrogen, with an appearance energy of 15.35 eV in naphthalene fragmentation,[48] plays a critical role on the surface in DLC formation from plasma enhanced CVD. Reaction of hydrogen atoms with CH bonds at the surface can lead to the formation of dangling bonds on the surface. Frequently, these radical sites are refilled with hydrogen by combining with gaseous atomic hydrogen. However, the constant turnover of surface hydrogen drives the surface chemistry and results in the dehydrogenation of adsorbed carbon containing molecules and the addition of carbon to the lattice. Also, hydrogen can react with any carbon sp^1 or sp^2 sites on the surface converting them into sp^3 bonded carbon during this turnover. Beneath the surface, hydrogen can penetrate into the bulk, due to its size, where they can abstract hydrogen from a CH bond and create subsurface dangling bonds and molecular hydrogen, which desorbs from the bulk. The dangling bonds can then preferentially form sp^3 bonds.[28]

VI. CONCLUSION AND OUTLOOK

Nano-diamond-like-carbon has been formed from UV multi-photon excitation of naphthalene in a static gas cell, with sp^3/sp^2 ratio of ca. 8.1. To our knowledge this is the first report on the formation of DLC from photo-excitation of molecules in the gas phase, and from UV excitation of a hydrocarbon (irrespective of the phase). The technique enables a new way to study diamond formation *in situ*. However, under the current experimental conditions, the time resolution is not sufficiently high to observe the chemical/physical pathways to formation. Optical access to the molecular assortment is obtainable for other *in situ* spectroscopic techniques with higher time resolution, such as laser-induced fluorescence or resonance-enhanced multi-photon excitation.[57] The high spatial resolution of such techniques may also provide valuable information as to the source of the transport features observed. The work presented here may be of significant interest for astro-chemists concerning the UV photo-excitation of polycyclic aromatic hydrocarbons (which are believed to be abundant in the interstellar medium[58,59]), and the possible pre-solar formation of NDs observed in meteorites develops through a chemical pathway.[60] Although the density and temperature in the experiments outlined here differ substantially from those in the interstellar medium, the results suggest that NDs can indeed be formed in the gas phase through a chemical pathway.

The physical process of agglomeration of nanoparticles was observed over successive measurements following their initial chemical formation. Their optical properties were modeled on a porous DLC material, with the refractive index estimated using the Bruggeman effective medium approximation. The porosity of the material was chosen from the ballistic particle cluster aggregates model, with a filling factor of 0.85, of Kozasa *et al.*[45] Their size-distribution was modeled using a log-normal distribution and particles with diameters in excess of ca. 650 nm were observed in very low concentrations. The highest sources of extinction were from particles of diameters between 125 and 350 nm. Agglomeration of DLC particles in the gas phase is an important deterrent in many forms of ND synthesis, such as detonation synthesis, where agglomerates with sizes in the order of microns have been observed.

Further analysis and investigation of this novel production method of ND materials from nanosecond UV light pulses focused into a gaseous mixture of a polycyclic aromatic hydrocarbon and helium are likely to have impact in many fields of science and technology.

ACKNOWLEDGMENTS

[1]V. N. Mochalin, O. Shenderova, D. Ho, and Y. Gogotsi, "The properties and applications of nanodiamonds," Nat. Nanotechnol. **7**, 11–23 (2012).

[2]"NATO science series," in *Synthesis, Properties and Applications of Ultra-nanocrystalline Diamond*, edited by D. M. Gruen, O. A. Shenderova, and A. Y. Vul' (Springer, Netherlands, 2005).

[3]A. Krüger, "Diamond nanoparticles: Jewels for chemistry and physics," Adv. Mater. **20**, 2445–2449 (2008).

[4]A. Shakun, J. Vuorinen, M. Hoikkanen, M. Poikelispaa, and A. Das, "Hard nanodiamonds in soft rubbers: Past, present and future—A review," Composites, Part A **64**, 49–69 (2014).

[5]K. V. Purtov, A. I. Petunin, A. E. Burov, A. P. Puzyr, and V. S. Bondar, "Nanodiamonds as carriers for address delivery of biologically active substances," Nanoscale Res. Lett. **5**, 631–636 (2010).

[6]X. Q. Zhang, R. Lam, X. Y. Xu, E. K. Chow, H. J. Kim, and D. Ho, "Multimodal nanodiamond drug delivery carriers for selective targeting, imaging, and enhanced chemotherapeutic efficacy," Adv. Mater. **23**, 4770–4775 (2011).

[7]*Ultrananocrystalline Diamond: Synthesis, Properties, and Applications* edited by O. A. Shenderova and D. M. Gruen (William Andrew Publishing, New York, USA, 2006).

[8]N. A. Kotov, "Inorganic nanoparticles as protein mimics," Science **330**, 188–189 (2010).

[9]O. A. Shenderova, V. V. Zhirnov, and D. W. Brenner, "Carbon nanostructures," Crit. Rev. Solid State Mater. Sci. **27**, 227–356 (2002).

[10]J. R. Maze, P. L. Stanwix, J. S. Hodges, S. Hong, J. M. Taylor, P. Cappellaro, L. Jiang, M. V. G. Dutt, E. Togan, A. S. Zibrov, A. Yacoby, R. L. Walsworth, and M. D. Lukin, "Nanoscale magnetic sensing with an individual electronic spin in diamond," Nature **455**, 644–648 (2008).

[11]J. Tisler, R. Reuter, A. Lammle, F. Jelezko, G. Balasubramanian, P. R. Hemmer, F. Reinhard, and J. Wrachtrup, "Highly efficient FRET from a single nitrogen-vacancy center in nanodiamonds to a single organic molecule," ACS Nano **5**, 7893–7898 (2011).

[12]Y. R. Chang, H. Y. Lee, K. Chen, C. C. Chang, D. S. Tsai, C. C. Fu, T. S. Lim, Y. K. Tzeng, C. Y. Fang, C. C. Han, H. C. Chang, and W. Fann, "Mass production and dynamic imaging of fluorescent nanodiamonds," Nat. Nanotechnol. **3**, 284–288 (2008).

[13]A. P. Jones and L. B. d'Hendecourt, "Interstellar nanodiamonds," in *Astrophysics of Dust*, edited by A. N. Witt, G. C. Clayton, and B. T. Draine (Astronomical Society of the Pacific, Estes Park, CO, USA, 2004).

[14]H. Mutschke, A. C. Andersen, C. Jäger, T. Henning, and A. Braatz, "Optical data of meteoritic nano-diamonds from far-ultraviolet to far-infrared wavelengths," Astron. Astrophys. **423**, 983–993 (2004).

[15]A. Virag, E. Zinner, R. S. Lewis, and M. Tang, "Isotopic compositions of H, C, and N in C diamonds from the Allende and Murray carbonaceous chondrites," in *Abstracts of the Lunar and Planetary Science Conference* (1989), Vol. 20, pp. 1158–1159.

[16]M. Baidakova and A. Vul', "New prospects and frontiers of nanodiamond clusters," J. Phys. D: Appl. Phys. **40**, 6300–6311 (2007).

[17]A. I. Lymkin, E. A. Petrov, A. P. Ershov, G. V. Sakovitch, A. M. Staver, and V. M. Titov, "Production of diamonds from explosives," Dokl. Akad. Nauk USSR **302**, 611–613 (1988).

[18]B. P. Tolochko, V. M. Titov, A. P. Chernyshev, K. A. Ten, E. R. Pruuel, I. L. Zhogin, P. I. Zubkov, N. Z. Lyakhov, L. A. Lukyanchikov, and M. A. Sherornov, "Physical-chemical model of processes at detonation synthesis of nanodiamonds," Diamond Relat. Mater. **16**, 2014–2017 (2007).

[19]K. Niwase, T. Tanaka, Y. Kakimoto, K. N. Ishihara, and P. H. Shingu, "Raman spectra of graphite and diamond mechanically milled with agate or stainless-steel mall-mill," Mater. Trans., JIM **36**, 282–288 (1995).

[20]G. W. Yang, J. B. Wang, and Q. X. Liu, "Preparation of nano-crystalline diamonds using pulsed laser induced reactive quenching," J. Phys.: Condens. Matter **10**, 7923–7927 (1998).

[21]M. Frenklach, R. Kematick, D. Huang, W. Howard, K. E. Spear, A. W. Phelps, and R. Koba, "Homogeneous nucleation of diamond powder in the gas-phase," J. Appl. Phys. **66**, 395–399 (1989).

[22]D. G. Goodwin and J. E. Butler, "Theory of diamond chemical vapor deposition," in *Handbook of Industrial Diamonds and Diamond Films*, edited by M. A. Prelas, G. Popovici, and L. K. Bigelow (CRC Press, New York, 1997), pp. 527–581.

[23]G. Burkhard, H. Tamura, Y. Tanabe, A. B. Sawaoka, and K. Yamada, "Formation of diamond during passage of a shock-wave in a copper graphite powder—Formation process and numerical simulation," Appl. Phys. Lett. **66**, 3131–3133 (1995).

[24]O. N. Fedyanina and P. N. Nesterenko, "Regularities of chromatographic retention of phenols on microdispersed sintered detonation nanodiamond in aqueous-organic solvents," Russ. J. Phys. Chem. A **84**, 476–480 (2010).

[25]H. Huang, E. Pierstorff, E. Osawa, and D. Ho, "Active nanodiamond hydrogels for chemotherapeutic delivery," Nano Lett. **7**, 3305–3314 (2007).

[26]A. Krüger, F. Kataoka, M. Ozawa, T. Fujino, Y. Suzuki, A. E. Aleksenskii, A. Y. Vul', and E. Osawa, "Unusually tight aggregation in detonation nanodiamond: Identification and disintegration," Carbon **43**, 1722–1730 (2005).

[27]S. A. Alterovitz, N. Savvides, F. W. Smith, and J. A. Woollam, "Amorphous hydrogenated 'diamondlike' carbon films and arc-evaporated carbon films," in *Handbook of Optical Constants of Solids II*, edited by E. D. Palik (Academic Press, London, 1991).

[28]J. Robertson, "Diamond-like amorphous carbon," Mater. Sci. Eng., R **37**, 129–281 (2002).

[29]A. A. Ruth, E. W. Gash, M. Staak, and S. E. Fiedler, "Multi-photon UV photolysis of naphthalene gas mixtures: A new oscillatory system," Phys. Chem. Chem. Phys. **4**, 5217–5220 (2002).

[30]A. J. Walsh, A. A. Ruth, E. W. Gash, and M. W. D. Mansfield, "Multi-photon UV photolysis of gaseous polycyclic aromatic hydrocarbons: Extinction spectra and dynamics," J. Chem. Phys. **139**, 054304 (2013).

[31]S. E. Fiedler, A. Hese, and A. A. Ruth, "Incoherent broadband cavity enhanced absorption spectroscopy," Chem. Phys. Lett. **371**, 284–294 (2003).

[32]E. W. Gash, Ph.D. thesis, University College Cork, Cork, Ireland, 2004, pp. 75–183.

[33]C. F. Bohren and D. R. Huffman, *Absorption and Scattering of Light by Small Particles* (John Wiley and Sons, New York, 1983).

[34]Wolfram Research, Inc., Mathematica, version 8.0, Champaign, IL, 2010.

[35]H. Wang, "Formation of nascent soot and other condensed-phase materials in flames," Proc. Combust. Inst. **33**, 41–67 (2011).

[36]M. Frenklach, "Reaction mechanism of soot formation in flames," Phys. Chem. Chem. Phys. **4**, 2028–2037 (2002).

[37]H. Chang and T. T. Charalampopoulos, "Determination of the wavelength dependence of refractive indices of flame soot," Proc. R. Soc. A **430**, 577–591 (1990).

[38]C. Jäger, H. Mutschke, and T. Henning, "Optical properties of carbonaceous dust analogues," Astron. Astrophys. **332**, 291–299 (1998).

[39]N. Savvides, "Ion-assisted deposition and metastable structures," Thin Solid Films **163**, 13–32 (1988).

[40]N. Savvides, "Low energy ion-assisted deposition of a–C:H films; a study of optical parameters with increasing hydrogenation," in *Amorphous Hydrogenated Carbon Films*, edited by P. Koidl and P. Oelhafen (Les Editions de Physique, Paris, 1987), p. 275.

[41]N. Savvides, "Optical constants and associated functions of metastable diamondlike amorphous carbon films in the energy range 0.5–7.3 eV," J. Appl. Phys. **59**, 4133–4145 (1986).

[42]J. Tauc, "Optical properties and electronic structure of amorphous Ge and Si," Mater. Res. Bull. **3**, 37–46 (1968).

[43]J. Yon, F. Liu, A. Bescond, C. Caumont-Prim, C. Rozé, F. Ouf, and A. Coppalle, J. Quant. Spectrosc. Radiat. Transfer **133**, 374–381 (2014).

[44]D. A. G. Bruggeman, "Berechnung verschiedener physikalischer Konstanten von heterogenen Substanzen. I. Dielektrizitätskonstanten und Leitfähigkeiten der Mischkörper aus isotropen Substanzen," Ann. Phys. **416**, 636–664 (1935).

[45]T. Kozasa, J. Blum, and T. Mukai, "Optical properties of dust aggregates. I. Wavelength dependence," Astron. Astrophys. **263**, 423–432 (1992).

[46]C. H. van der Bogert, C. P. Smith, T. Hainschwang, and S. F. McClure, "Gray-to-blue-to-violet hydrogen-rich diamonds from the argyle mine, Australia," Gems Gemol. **45**, 20–37 (2009).

[47]C. H. van der Bogert, C. P. Smith, T. Hainschwang, and S. F. McClure, "Photoluminescencestudy of hydrogen-rich gray-to-blue-to-violet diamonds from the Argyle mine, Australia," in *Conference on Micro-Raman Spectroscopy and Luminescence Studies in the Earth and Planetary Sciences, 2–4 April, Mainz, Germany*, LPI Contribution No. 1473 (American Institute of Physics, 2009), pp. 87–88.

[48]J. Zhen, P. Castellanos, D. M. Paardekooper, N. Ligterink, H. Linnartz, L. Nahon, C. Joblin, and A. G. G. M. Tielens, "Laboratory photo-chemistry of PAHs: Ionization versus fragmentation," Astrophys. J. Lett. **804**, L7 (2015).

[49]J. Zhen, S. Rodriguez Castillo, C. Joblin, G. Mulas, H. Sabbah, A. Giuliani, L. Nahon, S. Martin, J.-P. Champeaux, and P. M. Mayer, "VUV photo-processing of PAH cations: Quantitative study on the ionization versus fragmentation processes," Astrophys. J. **822**, 113 (2016).

[50]H. W. Jochims, H. Rasekh, E. Ruhl, H. Baumgärtel, and S. Leach, "The photofragmentation of naphthalene and azulene monocations in the energy range 7–22 eV," Chem. Phys. **168**, 159–184 (1992).

[51]H. W. Jochims, E. Rühl, H. Baumgärtel, S. Tobita, and S. Leach, "Size effects on dissociation rates of polycyclic aromatic hydrocarbon cations laboratory studies and astrophysical implications," Astrophys. J. **420**, 307–317 (1994).

[52]Y. Gotkis, M. Oleinikova, M. Naor, and C. Lifshitz, "Time-dependent mass spectra and breakdown graphs. 17. Naphthalene and phenanthrene," J. Phys. Chem. **97**, 12282–12290 (1993).

[53]R. J. Van Brunt and M. E. Wacks, "Electron-impact studies of aromatic hydrocarbons. III. Azulene and naphthalene," J. Chem. Phys. **41**, 3195–3199 (1964).

[54]S. P. Ekern, A. G. Marshall, J. Szczepanski, and M. Vala, "Photodissociation of gas-phase polycyclic aromatic hydrocarbon cations," J. Phys. Chem. A **102**, 3498–3504 (1998).

[55]K. H. Homann, "Formation of large molecules, particulates and ions in premixed hydrocarbon flames; Progress and unresolved questions," Symp. (Int.) Combust., [Proc.] **20**, 857–870 (1985).

[56]V. V. Danilenko, *Nanocarbon Phase Diagram and Conditions for Detonation Nanodiamond Formation* (Springer, Dordrecht, 2005).

[57]J. M. Hollas, *Modern Spectroscopy* (John Wiley & Sons, Chichester, 2004).

[58]A. G. G. M. Tielens, "Interstellar polycyclic aromatic hydrocarbon molecules," Annu. Rev. Astron. Astrophys. **46**, 289–337 (2008).

[59]A. G. G. M. Tielens, "The molecular universe," Rev. Mod. Phys. **85**, 1021–1081 (2013).

[60]C. Le Guillou, J. N. Rouzaud, L. Remusat, A. Jambon, and M. Bourot-Denise, "Structures, origin and evolution of various carbon phases in the ureilite Northwest Africa 4742 compared with laboratory-shocked graphite," Geochim. Cosmochim. Acta **74**, 4167–4185 (2010).

[61]There is no general consensus on the terminology of DLC and a–(C:H).[27] We will use DLC in the context of this publication to refer to both diamond containing a fraction of graphite, and/or hydrogenated amorphous carbon.